A SPIN MANIPULATOR FOR ELECTRON ACCELERATORS

D. A. Engwall, B. M. Dunham, and L. S. Cardman
Nuclear Physics Laboratory, Department of Physics,
University of Illinois at Urbana-Champaign,
Champaign, Illinois, 61820

D. P. Heddle
Department of Physics and Computer Science,
Christopher Newport University,
Newport News, Virginia, 23606
and
Continuous Electron Beam Accelerator Facility,
Newport News, Virginia, 23606

and

C. K. Sinclair
Continuous Electron Beam Accelerator Facility,
Newport News, Virginia, 23606

June 12, 1992

Abstract

We have designed and constructed a novel optical system capable of manipulating the orientation of the polarization direction, $\vec{P}$, of a 100 keV beam of polarized electrons relative to the momentum vector, $\vec{k}$, in an arbitrary manner. This spin manipulator is fully compatible with the UHV requirements of the photocathode sources that are typically used for accelerator-based experiments involving polarized electrons. We describe the design and operation of the system and its components, and document its performance.

1 Introduction

Most experiments of interest involving the scattering of high energy electrons require [1] the spin of the electron to be longitudinal at the position of the scattering target. Most polarized electron sources (see, eg. [2], and references therein) are based on photoemission from semiconductors (usually GaAs and related compounds). The electrons emitted by these sources have longitudinal polarization, but if there are any net deflections in the beam transport between the source and the experimental apparatus, the polarization vector, $\vec{P}$, will precess relative to the electron momentum, $\vec{k}$, and no longer be longitudinal at the target position. So long as all of the electrons in the beam pass through *the same* magnetic fields on their way from the source to the target and effects associated with the finite phase volume of the beam are negligible, it is possible to provide a beam that maintains its polarization from the source to the target, and to compensate for the precession in the transport system by installing a spin manipulator that operates on the beam either at the injector to the accelerator or just before the target. Since spin manipulation at injection energies is much easier than spin manipulation at accelerator output energies, the former approach is preferred whenever it is possible. It is the approach we have taken in planning for spin manipulation at the 4 GeV CEBAF accelerator, where the injection energy is 100 keV.

A spin manipulator has a number of uses beyond permitting one to achieve the desired longitudinal polarization at the target location. If one is able to orient the spin arbitrarily at the target location it is possible to check for systematic errors in the spin transport properties of the beam transport system and for polarization-related effects in the experimental apparatus, such as sensitivity to transverse polarization. A spin manipulator also provides an independent check of the "standard" technique for reversing the helicity of the electron beam: reversing the sense of circular polarization of the laser driving the photocathode source. Finally, Mott scattering at the injection energy of 100 keV provides a convenient technique for characterizing the performance of a polarized electron source. Mott scattering polarimetry requires that the beam have completely transverse polarization oriented "up" and then "down" with respect to the scattering plane, so spin manipulation is required before we can use this technique.

This paper is organized as follows. First, in Section 2, we review briefly three possible designs for beam transport systems capable of performing a completely general spin manipulation: a rotating Wien filter; a Wien filter followed by a solenoidal rotator; and a pair of electrostatic bends separated by a solenoidal rotator and followed by a second solenoidal rotator. The third approach, which we shall refer to as the "Z" manipulator in reference to its layout, was used for the spin manipulator whose design and construction is described in detail in this paper. In Section 3 we review the effects of various beamline components on spin precession, and then explain in detail the spin precession in the "Z" manipulator design. In Section 4 we examine the sensitivities of the spin precession in the manipulator to changes in the beam energy and to mis- settings of the fields in the various components. Next, in Section 5, we discuss the transverse optical characteristics

of the manipulator. Then in Section 6 we discuss the mechanical and electrical realization of the electrostatic bends and solenoids in the manipulator that we constructed. Its operation and performance is documented in Section 7. Finally, in Section 8, we present our conclusions.

The spin manipulator we have constructed is designed for use in conjunction with a polarized electron source that operates at 100 keV. Any numerical results presented in this paper apply specifically to this energy.

2 Spin Manipulation Techniques

The simplest technique for manipulation of the orientation of the spin direction of a polarized electron beam is to employ a Wien filter that can be rotated mechanically about the beam axis. A Wien filter [3] consists of crossed $\vec{E}$ and $\vec{B}$ fields that are perpendicular to the particle direction and whose relative strength has been adjusted so that the central ray of the electron beam experiences no transverse force. The spin vector of the beam precesses about the $\vec{B}$ field in a Wien filter due to the torque arising from the interaction of the spin with the magnetic field. The electron polarization vector, $\vec{P}$, of a longitudinally polarized beam can be rotated to an arbitrary opening angle, θ, with respect to the beam direction, $\vec{k}$, by setting the integral $\int B_\perp \, dl$ of the perpendicular magnetic field along the axis of the Wien filter to the appropriate value.

It is also possible to choose the azimuthal angle, ϕ, of the spin vector with respect to the beam direction by mechanically rotating the Wien filter about the beam axis since the spin precession will be about the direction defined by the $\vec{B}$ field. This approach, while often used, for example, in conjunction with polarized proton sources, is not appropriate for photocathode-based polarized electron sources such as the one built for CEBAF because of the ultra high vacuum (UHV) requirements of these sources.

A slightly more complex approach that has no rotating parts, and is therefore easier to realize in a UHV beamline, involves the use of a Wien filter followed by a solenoidal rotator, as shown schematically in Figure 1a. In this design, hereafter referred to as the "W & S" manipulator, the orientation of the Wien filter is fixed, so it can define θ in a single plane. The axial field in the rotator is then adjusted to precess the spin direction from the ϕ-value of the plane defined by the Wien filter (typically 0 or 90°) to the desired final value.

An alternate approach is the "Z" configuration of electrostatic bends and solenoids shown in Figure 1b. This method of spin manipulation was first suggested by Reichert [4, 5]. Unlike the "W & S" approach, the "Z" spin manipulator uses solenoidal precession for both the polar and azimuthal rotations. Discussion of its operation is postponed to Section 3.2. The transverse optics of the "Z" design are more easily controlled than those of the "W & S" design. In addition, this design permits the inclusion of a Mott polarimeter as

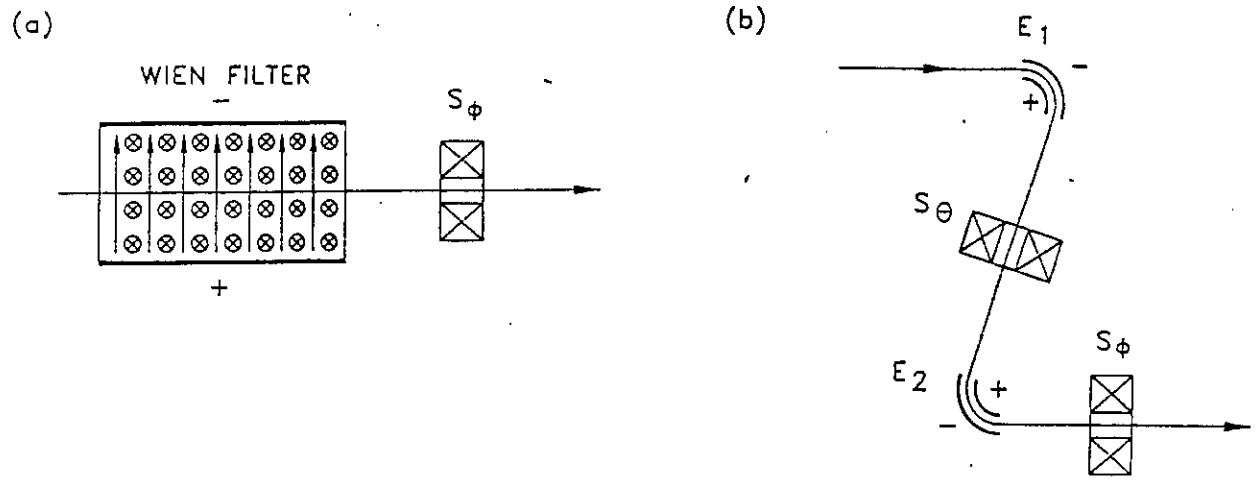

Figure 1: A schematic representation of two design approaches to a spin manipulator: (a) the Wien filter plus a solenoidal rotator; and (b) the "Z" configuration, which consists of a pair of electrostatic bends with a solenoidal rotator between them and a second solenoidal rotator following them.

a permanent part of the beamline (permitting rapid checks on the performance of the source), and its geometry provides excellent vacuum isolation between the polarized source and the accelerator.

3 Spin Transport in the "Z" Manipulator

In order to understand the design and operation of the "Z" spin manipulator, we first review the spin transport characteristics of electrostatic bends and solenoids. Then we apply these results to explain the operation of the "Z" spin manipulator.

3.1 Spin Transport Through the Components of the "Z" Spin Manipulator

In this section we describe the effects on the electron polarization vector of each of the components used in the spin manipulator. We use the traditional TRANSPORT [6] notation, for describing the beam, and the polar angles, θ and ϕ, for describing the orientation of the polarization vector, $\vec{P}$, relative to the beam direction, as shown in Figure 2. In this coordinate system the $\hat{z}$ unit vector always points in the beam direction (i.e. along the beam momentum vector, $\vec{k}$), the $\hat{x}$ unit vector lies in the bend plane, and the $\hat{y}$ unit vector is perpendicular to the bend plane.

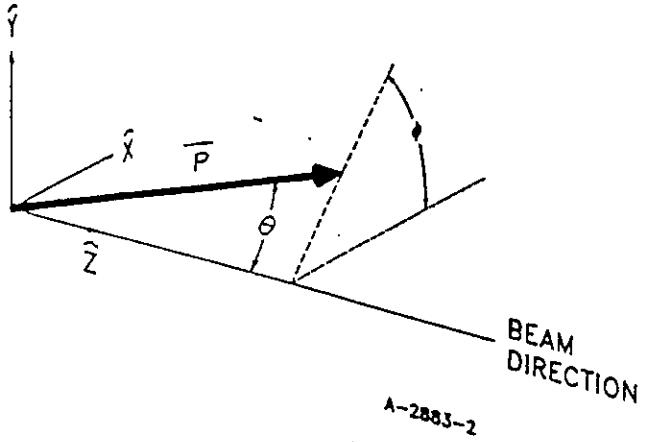

Figure 2: The coordinate system used for describing the beam, and the angles, θ and ϕ, that describe the orientation of the polarization vector, $\vec{P}$, relative to the beam direction.

3.1.1 The Electrostatic Bend

First we consider an electrostatic bend. This element uses a static electric field $\vec{E}$, transverse to the beam trajectory, to bend the electron beam through some angle θ_b. This also causes the electron polarization vector to rotate. The angle η_e by which the longitudinal component of the polarization vector precesses with respect to the central beam axis is given by [7]:

$$\eta_e = \left(\frac{g}{2\gamma} - a\gamma\right)\theta_b, \tag{1}$$

where a is the gyromagnetic anomaly, $g/2 - 1 = 0.00115965$, and $\gamma = (1 - v^2/c^2)^{-\frac{1}{2}}$ is the usual relativistic factor, with v the electron velocity. The sense of the polarization rotation is given by the right hand rule and the fact that $\vec{\eta}_e$ lies in the direction of $-q\vec{v} \times \vec{E}$, where q is the electron charge, $-e$. For example, the first electrostatic bend of the spin manipulator has $(-q/e)\hat{v} \times \hat{E} = \hat{y}$, so it rotates the polarization about $\hat{y}$ from $\hat{z}$ toward $\hat{x}$. In the non-relativistic limit, $\gamma \to 1$, and $\eta_e \to \theta_b$, so a 90° electrostatic bend would precess the spin from longitudinal to transverse. The "Z" manipulator discussed here was designed for operation at 100 keV, where $\gamma = 1.196$. Substituting this value in Equation (1) indicates that a 107.7° bend is required to precess the spin from longitudinal to transverse at 100 keV.

3.1.2 The Solenoid

Next we consider the solenoid. This element operates by producing a longitudinal, static magnetic field $\vec{B}$ which is either parallel or antiparallel to the electron trajectory. This causes the transverse component of the polarization vector to precess [7] about the beam

axis by an angle η_s:

$$\eta_s = \frac{geBL_s}{2mv\gamma}. \tag{2}$$

Here BL_s is just the integral $\int B_z\, dl$ of the axial field along the axis of the solenoid, m is the electron mass, and the other symbols have been defined above. The sense of the polarization rotation is again given by the right hand rule and the fact that $\vec{\eta}_s$ lies in the direction of $\vec{B}$. For example, if the solenoid following the Wien filter in Figure 1a has $\hat{B} = \hat{z}$, then it rotates the polarization from $\hat{x}$ toward $\hat{y}$, changing the azimuthal angle, ϕ, of the polarization vector by an amount η_s.

3.2 Spin Precession in the "Z" Spin Manipulator

Now consider a generalized spin manipulation apparatus of the type shown in Figure 1b for the case in which the incident beam has purely longitudinal polarization. The first electrostatic bend rotates the longitudinal component of the initial beam polarization vector, $\vec{P}_0$ by η_e about the $\hat{y}$ direction, resulting in the polarization vector, $\vec{P}_1$. Next, the first solenoidal rotator, S_θ, rotates the transverse component of $\vec{P}_1$ after the first bend by η_θ about the $\hat{z}$ direction while leaving the longitudinal component unchanged, resulting in $\vec{P}_2$. The second electrostatic bend, which is taken to be identical to the first, rotates the longitudinal component of $\vec{P}_2$ by η_e about the $-\hat{y}$ direction, leaving the transverse component unchanged, resulting in $\vec{P}_3$. Finally, the second solenoidal rotator, S_ϕ, rotates the transverse component of $\vec{P}_3$ by η_ϕ in the $\hat{z}$ direction, leaving its longitudinal component unchanged.

Taking the initial direction of $\vec{P}$ to be along $\hat{z}$, i.e., longitudinal, it is straightforward but tedious to calculate the final polar and azimuthal angles for $\vec{P}$ at the exit of the manipulator, viz

$$\theta = \cos^{-1}\left(\sin^2\eta_e \cos\eta_\theta + \cos^2\eta_e\right) \tag{3}$$

and

$$\phi = \cos^{-1}\left\{\frac{\left[\cos\eta_\phi\left(\cos\eta_\theta - 1\right)\sin\eta_e\cos\eta_e - \sin\eta_\theta\sin\eta_\phi\sin\eta_e\right]}{\sin\theta}\right\}. \tag{4}$$

These equations simplify considerably if the angles of the electrostatic bends are chosen such that the spin precession, η_e, in each is exactly 90°, i.e. $\theta_b = 107.7°$ for a 100 keV electron beam. In this case the expressions for the polar and azimuthal angles become:

$$\theta = \eta_\theta \tag{5}$$

and

$$\phi = \begin{cases} \eta_\phi + 90° & \theta > 0 \\ \eta_\phi - 90° & \theta < 0 \end{cases}. \tag{6}$$

The "Z" spin manipulator is designed to take advantage of this simplification, which effectively decouples the setting of the two spin projection angles θ and ϕ. As indicated by

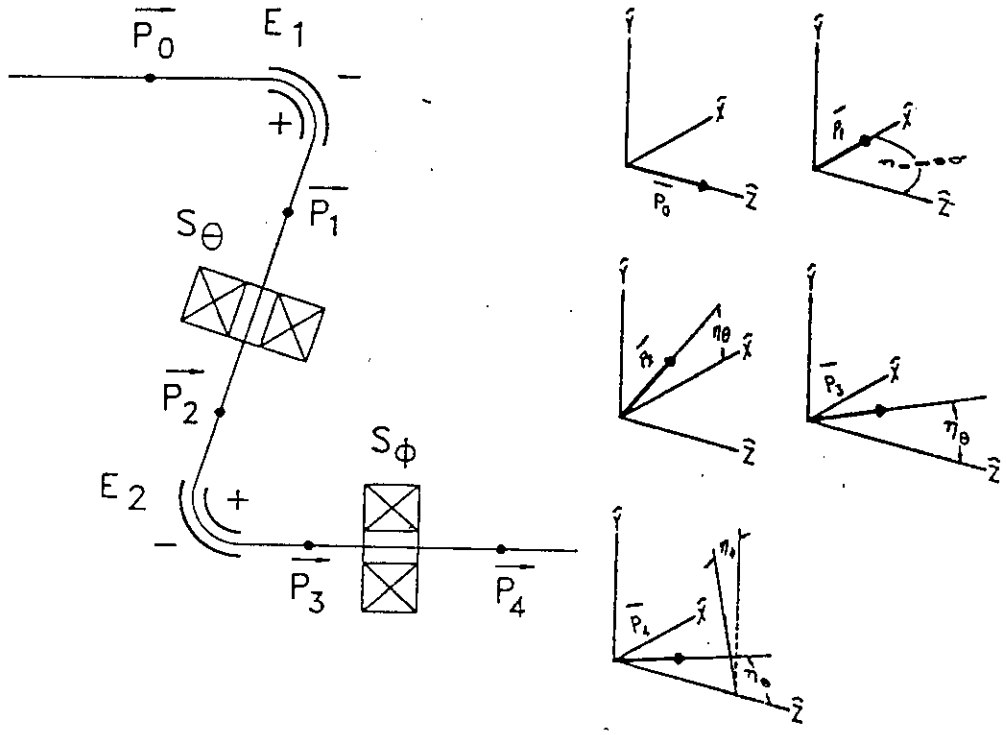

Figure 3: Orientation of the polarization vector $\vec{P}$ of an electron beam as it passes through the components of the "Z" spin manipulator. For the case shown, $\eta_\theta = 20°$, and $\eta_\phi = 15°$.

Equation (6), when S_ϕ is set for zero net precession, there is already an azimuthal precession of $\pm 90°$ (depending on the sign of θ) that arises from our definition of the coordinate system. Any rotation caused by S_ϕ is *in addition* to this initial value. The precession described above, for the case of $\eta_e = 90°$, is shown schematically in Figure 3.

4 Sensitivities of the Spin Precession to Errors

In this section we consider the sensitivity of the spin precession in the manipulator designs to two types of errors: fluctuations in the beam energy, $\delta E/E$, where E is the total energy of the beam ($E = T + m$, where T is the kinetic energy); and errors in setting the operating voltages and currents of the components in the manipulator. In analogy with the previous section, we begin with a consideration of the errors in the individual components, and then apply these results to the "Z" manipulator design.

4.1 Sensitivities in the Individual Components

4.1.1 The Electrostatic Bend

First consider the electrostatic bend. The spin precession as a function of the beam energy and bend angle are given by Equation (1). In order to calculate the sensitivity of the spin precession to the voltage difference, V, applied to the electrodes of the bend (i.e. the inner and outer electrodes are held at potentials of $+V/2$ and $-V/2$, respectively), we note that this voltage difference is inversely proportional to the radius of curvature ρ of the electron beam as it traverses the bend. This proportionality holds in the limit that the deviation in V is small enough that the electron beam travels close to the correct path, ensuring that the electric field remains orthogonal to the beam direction and the electrons are not accelerated by the electric field. In this case

$$\frac{\delta V}{V} = -\frac{\delta \rho}{\rho},$$

and

$$V\frac{\partial \eta_e}{\partial V} = -\rho\frac{\partial \eta_e}{\partial \rho} \tag{7}$$

$$= -\left(\frac{g}{2\gamma} - a\gamma\right)\rho\frac{\partial \theta_b}{\partial \rho}. \tag{8}$$

It is a straightforward but tedious exercise in trigonometry to show that this equation reduces to

$$V\frac{\partial \eta_e}{\partial V} = 0.456\,\frac{\text{deg}}{\%} \qquad (T = 100 \text{ keV and } \theta_b = 107.7°). \tag{9}$$

Next we evaluate the sensitivity of the electrostatic bend to error in the beam energy. From Equation (1) we obtain

$$E\frac{\partial \eta_e}{\partial E} = \gamma\frac{\partial \eta_e}{\partial \gamma} = -\left(\frac{g}{2\gamma} + a\gamma\right)\theta_b \tag{10}$$

$$= -0.9030\ \frac{\text{deg}}{\%} \qquad (T = 100 \text{ keV and } \theta_b = 107.7°). \tag{11}$$

4.1.2 The Solenoid

Noting that $m\gamma v = p = \sqrt{E^2 - m^2}$, we can rewrite Equation (2) for transverse spin precession in a solenoidal field as

$$\eta_s = \frac{geBL_s}{2\sqrt{E^2 - m^2}}. \tag{12}$$

Differentiating with respect to the beam energy E, then multiplying through by E, it is easy to obtain

$$E\frac{\partial \eta_s}{\partial E} = -\eta_s \frac{\gamma^2}{\gamma^2 - 1} = -\frac{\eta_s}{\beta^2} \tag{13}$$

$$= -0.03323\,\eta_s \;\frac{\text{deg}}{\%} \qquad (T = 100 \text{ keV}) \tag{14}$$

where, as usual, $\beta = v/c$.

To determine the sensitivity of the spin precession to the current in the solenoid we note simply that the field, B, in the solenoid is proportional to the current, I, that excites it. Therefore,

$$I\,\frac{\partial \eta_s}{\partial I} = B\,\frac{\partial \eta_s}{\partial B}\,. \tag{15}$$

Using Equation 2 we find:

$$I\,\frac{\partial \eta_s}{\partial I} = \frac{geBL}{2\gamma m v} \tag{16}$$

$$= 0.01\,\eta_s\,\frac{\text{deg}}{\%} \qquad (T = 100 \text{ keV}). \tag{17}$$

4.2 Sensitivities in the Complete Manipulator

The overall sensitivity of the "Z" spin manipulator to errors in the beam energy and in the settings of the electric and magnetic fields of the manipulator is complicated. One must perform an analysis on the composite precession results of Equation (3) and Equation (4) similar to what was done above for the individual components. The results obtained for the case of a 100 keV beam are summarized in Table 1. In calculating the sensitivity of the precession to the electrode voltage, V, we assumed that the two bends were connected in parallel, and that the electrodes in each bend were symmetrically positive and negative. The currents I_θ and I_ϕ refer to the currents in the solenoids, S_θ and S_ϕ, that set the final values of θ and ϕ, respectively. The quantity η_ϕ that appears in some of the table entries is related to ϕ by Equation 6. The sensitivities of the "W & S" style of spin manipulator were also investigated [8]; they were found to be comparable to those of the "Z" manipulator, so there is no reason to chose between the two designs on the basis of the sensitivities.

The overall accuracy of the "Z" manipulator for setting the desired spin direction can be estimated using the sensitivities presented in Table 1. It is straightforward to set the currents in the solenoids, the voltage on the electrodes of the bends, and the beam energies to an accuracy of ~0.1%. Taking these setting accuracies and adding the errors calculated using Table 1 linearly, we estimate that the overall accuracy in θ is

$$\delta\theta \simeq 0.0043 \;|\,\theta\,|\,. \tag{18}$$

Table 1: The sensitivities of the "Z" spin manipulator design to changes in the beam energy and to errors in the applied voltages and currents. All formulae are for $T = 100$ keV.

Parameter Varied	Sensitivity (degrees/%)	
	θ	ϕ
Beam Energy, E	$-0.033\,\theta$	$-0.033\,\eta_\phi + 0.90\left(\frac{1-\cos\theta}{\sin\theta}\right)$
Electrode Voltage, V	0	$0.46\left(\frac{\cos\theta-1}{\sin\theta}\right)$
Current, I_θ	$0.010\,\theta$	0
Current, I_ϕ	0	$0.010\,\eta_\phi$

The uncertainty is worst at $\theta = 180°$ where it becomes as large as 0.77°. The overall accuracy in ϕ is

$$\delta\phi \simeq 0.0043 \mid \eta_\phi \mid + 0.136 \mid (1 - \cos\theta)/\sin\theta \mid . \tag{19}$$

Note that this formula has a singularity at $\theta = 180°$ (because ϕ is not defined there). There are also differences between the error estimates and the actual errors that increase as $\theta \rightarrow 180°$ because of the increasing sensitivity of the actual spin direction to small changes in θ and ϕ; the formulae above typically overestimate the errors by about 25% at large angles. The estimated uncertainty stays $\lesssim 1°$ for $\theta \leq 165°$ when ϕ is small, and for $\theta \lesssim 150°$ for $\phi \approx 180°$. The error increases rapidly as $\theta \rightarrow 180°$; it reaches 3° by $\theta = 175°$. Fortunately the larger uncertainties present as θ increases to 180° are not important for most experiments as it is the total transverse component of the spin that matters, and this component is small (independent of ϕ) because $\theta \simeq 180°$. Furthermore, this orientation of the spin vector can be obtained with substantially reduced errors simply by flipping the helicity of the electron beam at the source and then operating the manipulator at settings corresponding to very small values of θ. The overall estimated errors in setting the spin direction are quite satisfactory for the experiments presently planned for CEBAF.

5 The Transverse Optical Properties of the Spin Manipulator

5.1 General Considerations

When the transverse optical properties of the spin manipulator designs are considered it quickly becomes obvious that the simple versions of the manipulators shown in Figure 1 are not practical; it is necessary to add additional magnetic elements to compensate for the variation in the transverse optical properties of the manipulators as the spin direction is varied. The need for these elements can be seen simply by noting that as the axial fields in the solenoids are adjusted to rotate the spin vector direction, the focal lengths of these lenses (which vary as $1/B^2$ in the thin-lens approximation) vary as well. In addition, the transverse optical properties of a Wien filter vary as the E and B fields are changed.

In both the "W & S" and "Z" designs these effects can be dealt with cleanly by replacing the simple solenoid rotators of Figure 1 with four-solenoid rotators, as shown in Figure 4 for the "Z" design. In each four-solenoid rotator the center pair of solenoids is adjusted as necessary to provide the spin precession required. The outer pair of solenoids is operated with equal but opposing fields, so they have no net effect on the spin direction ($\int B_z\, dl \equiv 0$); they are adjusted as necessary to compensate for the varying transverse optical properties of the central solenoid pair (and, in the case of the "W & S" rotator, for the varying properties of the Wien filter). In the remainder of this section we indicate how this refinement can be implemented for the "Z" spin manipulator design presented here.

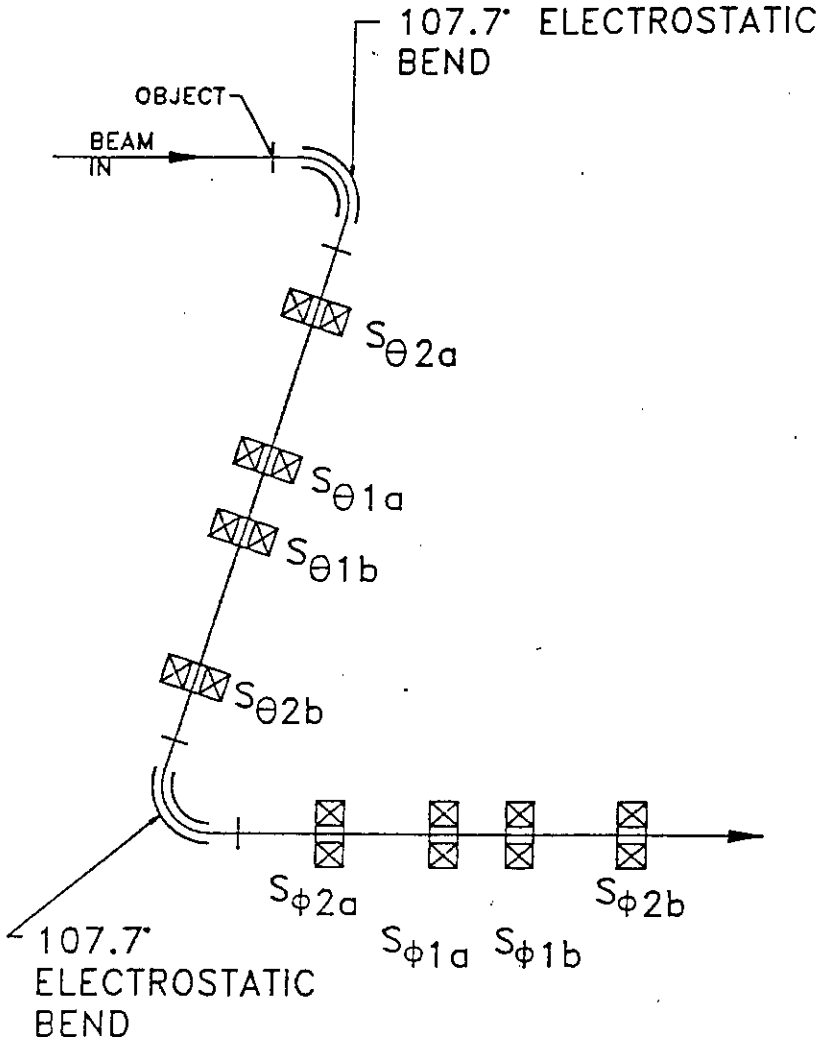

Figure 4: A practical realization of the "Z" spin manipulator. The single-solenoid rotators of Figure 1 have been replaced with four-solenoid rotators in which the outer pair adjust the transverse optical properties of the rotator while the center pair produces the spin precession.

In our intended application, the complete beam transport system from the photocathode of the polarized electron source through the injection line of the accelerator must be considered. The layout of the beamline is shown in Figure 5. The gun is mounted vertically, to simplify its construction and to facilitate easier operation. The beam is bent from vertical to horizontal in a small, 90° dipole with modest pole-face rotations. The first solenoid between the gun and the dipole is set to form a crossover in the middle of the dipole; this optical constraint plus the focusing effect of the pole face rotations suffice to yield equal beam size in both the horizontal and vertical directions after the bend, maintaining the initial symmetry of the beam. Two additional solenoids image the photocathode "spot" at the object point of the first electrostatic bend in the spin manipulator. Since the spin is longitudinal as it traverses these solenoids, they have no effect on the polarization vector.

The group of four solenoids between the electrostatic bends make up the θ-rotator since the precession they effect ultimately becomes the polar angle of the polarization vector $\vec{P}$. Similarly, we call the group of solenoids after the second electrostatic bend the ϕ-rotator, since they rotate ϕ from its initial value of $\pm 90°$ (after the second electrostatic bend) while leaving θ unaffected. The field integral through the solenoid pair $S_{\theta 1a}$ $S_{\theta 1b}$ is adjusted to provide the desired opening angle, θ, and the field integral through the solenoid pair $S_{\phi 1a}$ $S_{\phi 1b}$ is adjusted to provide the desired azimuthal angle, ϕ for the final spin direction. To compensate for the varying transverse optical characteristics of these lens pairs, the solenoids in both the $S_{\theta 2a}$ $S_{\theta 2b}$ and $S_{\phi 2a}$ $S_{\phi 2b}$ pairs are identical and "counterwound" so that they produce no net spin precession as their strength (and therefore their transverse optical properties) is varied.

First consider the θ-rotator; once the amount of rotation is chosen, the *sum* of field strengths for the solenoids performing the precession, $S_{\theta 1a}$ and $S_{\theta 1b}$, is fixed. This means that there are two degrees of freedom: $S_{\theta 2}$ (the common setting for the inversely coupled $S_{\theta 2a}$ $S_{\theta 2b}$ pair) and either $S_{\theta 1a}$ or $S_{\theta 1b}$. Our goal was to exploit these degrees of freedom to achieve common optical constraints for all values of θ. Similar considerations apply to the ϕ-rotator.

5.2 The θ-rotator

For the θ-rotator we utilized the two degrees of freedom to satisfy one precise optical constraint and one qualitative constraint. These will be discussed in turn. First, we note that the object and image points of the electrostatic bend are located symmetrically 10.3 cm upstream of the entrance and 10.3 cm downstream of the exit (both measured from the effective field boundary). The front-end optics produces a waist in both transverse directions at the object of the first electrostatic bend, which then images the waist at its image point. The θ-rotator is then required *for whatever value of θ has been chosen* to produce another waist at the entrance focal point of the second electrostatic bend.

The more qualitative constraint employed is that the principal rays are well behaved throughout the transport. In general, from those solutions that satisfied the waist-to-waist

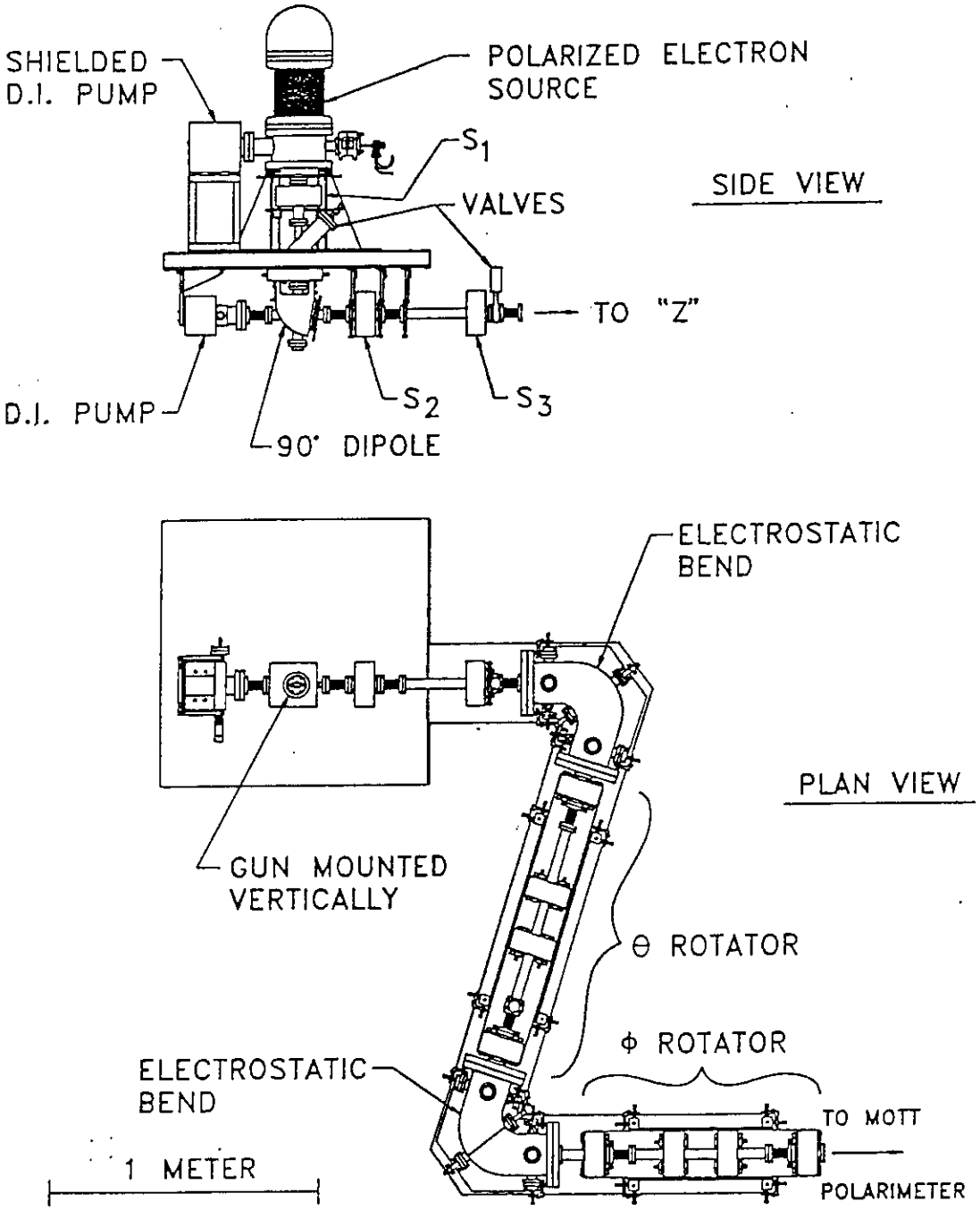

Figure 5: The Illinois/CEBAF 100 keV polarized electron source and its associated beamline. A side view of the region near the source itself is shown above a plan view of most of the beamline. Not shown are D.I. pumps located under each of the electrostatic bends and the viewscreen mechanisms and cameras that are used to observe the beam.

focussing requirement, the one with gentlest set of principal ray diagrams was selected. Beam envelopes and principal ray diagrams for a typical case of transport through the θ-rotator are presented in Figure 6.

5.3 The ϕ-rotator

The optical requirements for the ϕ-rotator are very similar to those discussed above for the θ-rotator; the ϕ-rotator is also required to provide waist-to-waist focussing (for all values of ϕ). The beginning of the ϕ rotator is the waist produced at the exit of the second electrostatic bend which is, in turn, the image of the waist produced at its entrance by the θ-rotator. For our application it was desired that the output waist for the ϕ rotator occur 31.8 cm after the exit of the last focussing solenoid ($S_{\phi 2b}$). As before, the qualitative constraint was to demand good behavior of the principal rays.

5.4 Beam Optical Properties of the "Z" Manipulator

In Figure 7 we show beam envelopes for transport through the spin-manipulator for several combinations of θ and ϕ. These diagrams show that we are able to achieve optical behavior which is basically independent of the desired spin projections. The small asymmetries observed in the beam envelopes result mainly from the fact that the off-diagonal elements of the TRANSPORT matrices describing the 90° dipole that precedes the manipulator are not identical.

6 Realization of the "Z" Spin Manipulator

In this section we outline the electrical, magnetic, and mechanical design of the components of our "Z" spin manipulator. We begin with a discussion of the 107.7° electrostatic bends, and then present the design of the solenoids.

6.1 The Electrostatic Bend

In order to bend an electron beam with an electrostatic field, we employed a radially-concentric toroidal condenser with field shunts at the entrance and exit (an electrostatic bend). In Figure 8, we show all the parameters needed to define such an electrostatic bend mechanically. In this section, we outline the design process, which was carried out analytically following the recommendations of Wollnik *et al* [9, 10], and we present the finished design.

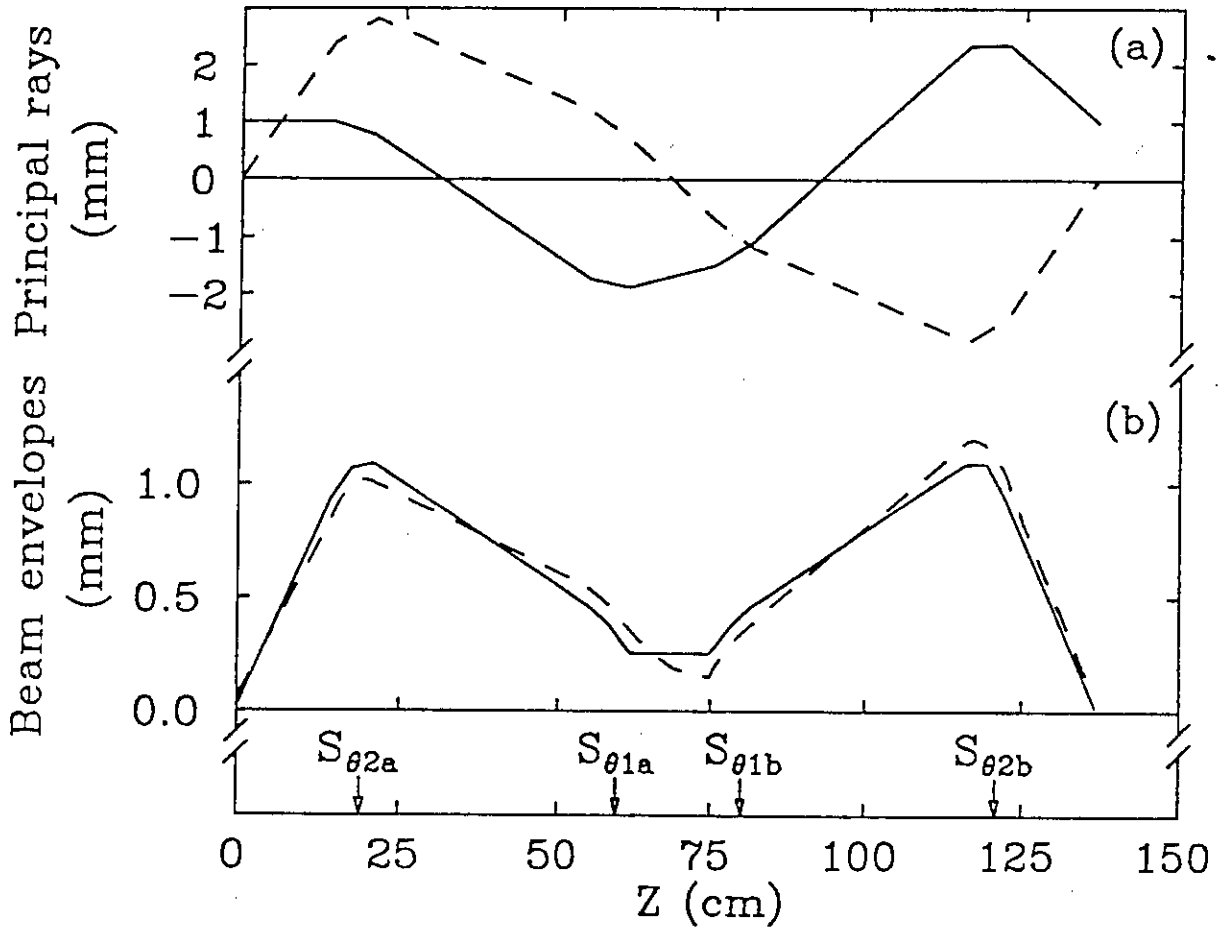

Figure 6: Principal ray diagrams (a) and beam envelopes (b) for a typical case of transport through the θ-rotator ($\theta = 90°$). The principal rays are for a 1 mm displacement (solid curve) and a 5 mr divergence (dashed curve), respectively. The envelopes shown are for both the horizontal (solid curve) and vertical (dashed curve) planes with the input beam phase volume that corresponds to the values calculated based on a TRANSPORT simulation of the beam from the photocathode to the entrance to the rotator.

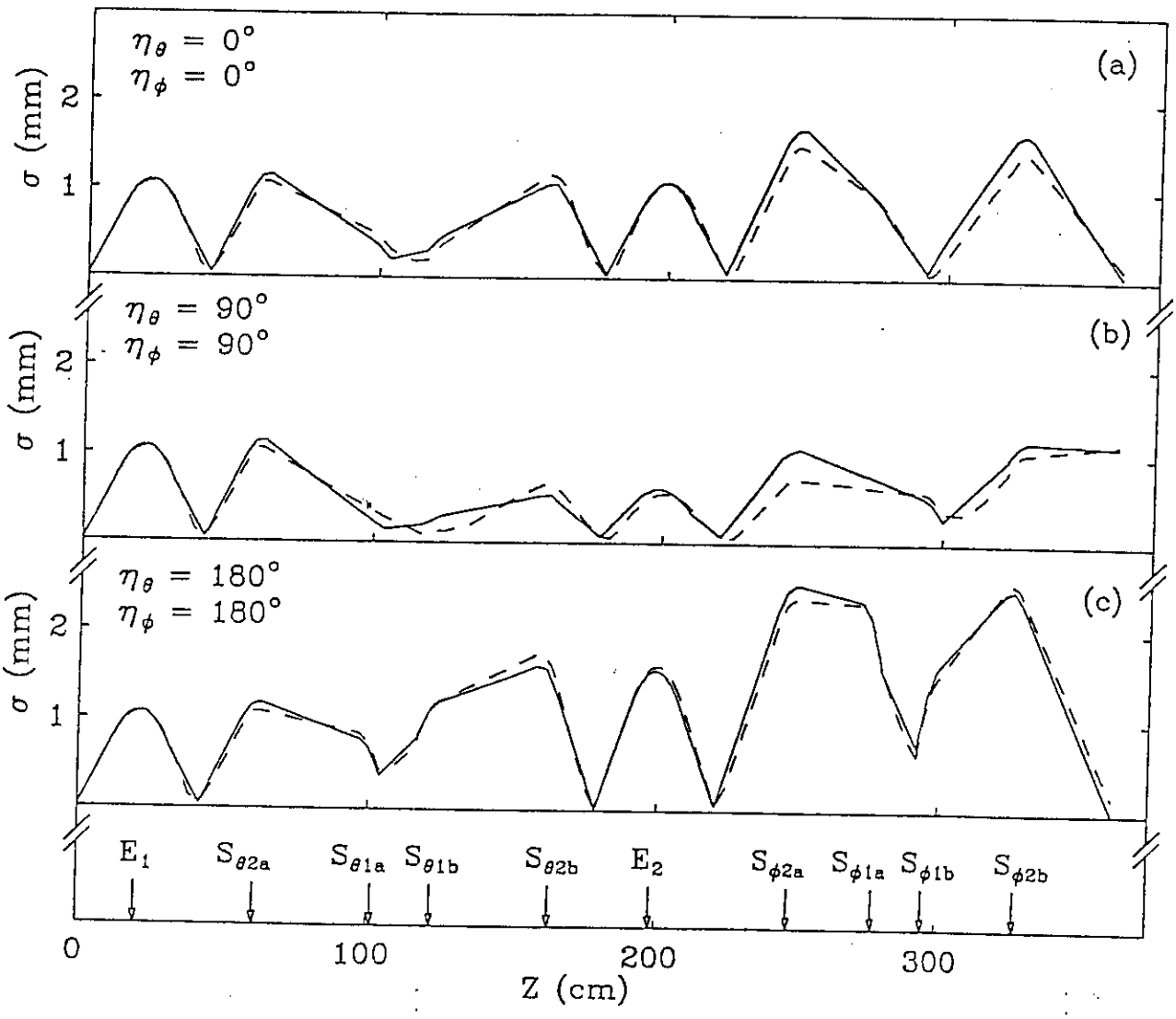

Figure 7: Transverse beam dimensions in the "Z" spin manipulator for several settings of the final spin direction: (a) $\theta = 0°$ and $\phi = 90°$; (b) $\theta = 90°$ and $\phi = 180°$; and (c) $\theta = 180°$ and $\phi = 270°$. The solid curves are the vertical beam dimension and the dashed curves are the horizontal beam dimension.

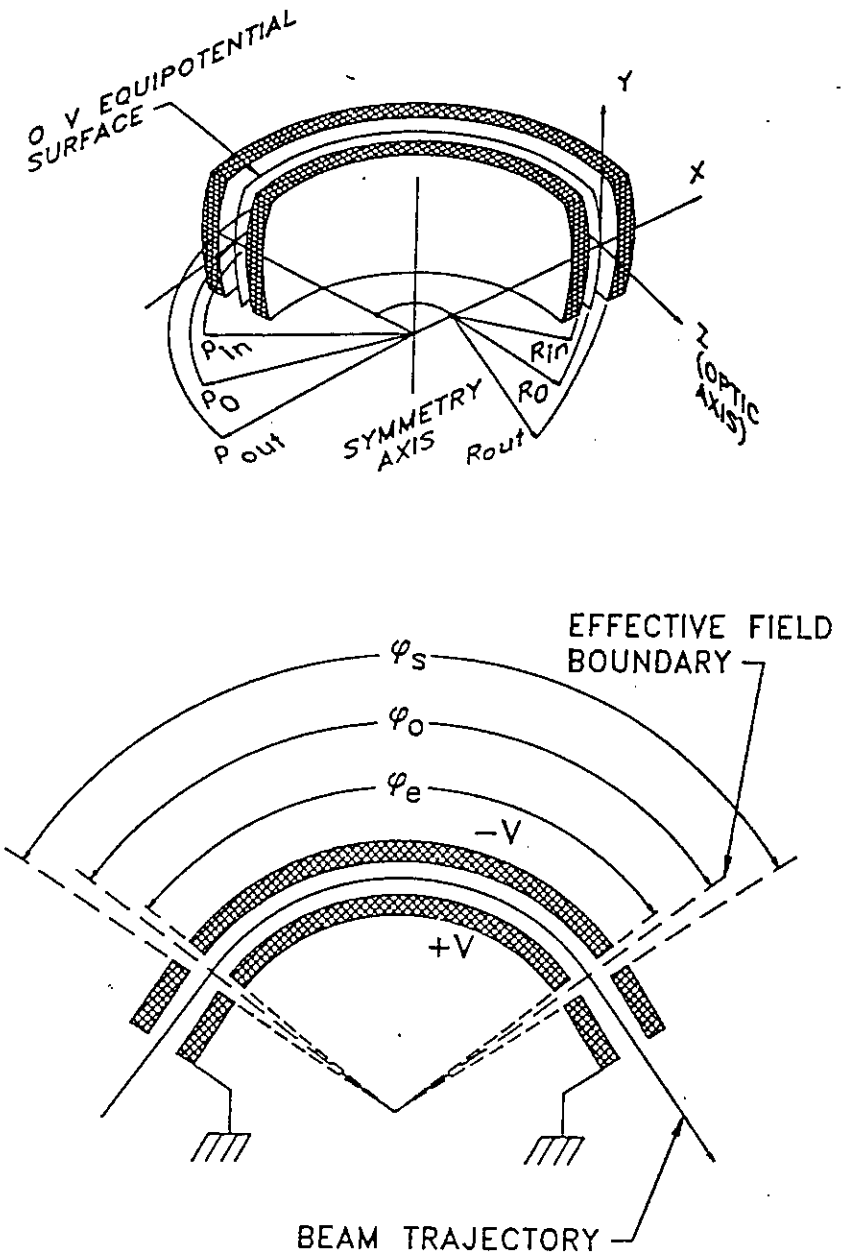

Figure 8: The geometrical parameters that define a toroidal electrostatic bend. The field shunts have been omitted from the upper figure for simplicity. The lower figure is a section through the bend plane.

6.1.1 Design Criteria

Four criteria were taken into account during the design process:

1. The 100 keV electron beam must be bent through an angle of 107.7° (which corresponds to a 90.0° spin precession at this energy).
2. The central ray in the electron beam must traverse the bend along the 0 V equipotential.
3. The electrostatic bend must be able to operate with a maximum voltage of +14 kV (−14 kV) maintained on the inner (outer) electrode. This allowed us to use inexpensive commercial power supplies.
4. The first-order optical properties of the bend in the x and y directions must be as similar as possible.

While the first three criteria are met easily, the last is more troublesome. As the electron beam passes through the fringe field region of the bend, it is defocussed only along the x direction [10]. This asymmetric defocussing prevents a perfect matching of the x and y optics. However, it is possible to approximate the desired optical symmetry closely.

6.1.2 Design Approach

In order to complete the design of the bend, we considered two things. First, we generated [9, 10] the usual, 4×4 sub-matrix of the first-order TRANSPORT matrix ($\mathcal{R}$) describing the transverse optical properties of the bend. This matrix describes the entire bend, including both the radially inhomogeneous sector fields and the two defocussing fringing fields. Then we adjusted the mechanical parameters of the bend within the constraints provided by the first three design criteria until the diagonal elements of the transfer matrix were equal. Consequently, we were able to arrive at values for all of the parameters required to define the electrostatic bend mechanically.

6.1.3 The Finished Design

The radius of curvature of the electron beam, ρ_0, is 11.081 cm in the final design for the electrostatic bend. This radius was a compromise between the improvements in the transverse optical properties of the bend with larger radius and the increased construction difficulties and "real- estate" requirements that come with larger radii. The inner electrode has a vertical radius of curvature of $R_{in} = 12.739$ cm and a horizontal radius of curvature of $\rho_{in} = 10.292$ cm. The outer electrode has a vertical radius of curvature of $R_{in} = 14.434$ cm

and a horizontal radius of curvature of $\rho_{in} = 11.987$ cm. The actual bend angle of $\varphi_0 = 107.7°$ is obtained by having the electrodes and the shunts subtend angles of $\varphi_e = 103.4°$ and $\varphi_s = 113.8°$, respectively. Finally, in keeping with the recommendations of reference [10], we note that the grounded, cylindrical shunts have a vertical radius of curvature equal to that of the 0 V equipotential surface: 13.528 cm.

In the interest of completeness, we list here the 4×4 submatrix that describes the first-order transverse optics of our electrostatic bend from effective field boundary to effective field boundary:

$$\mathcal{R} = \begin{pmatrix} -0.130 & 0.0116 & 0 & 0 \\ -84.8 & -0.130 & 0 & 0 \\ 0 & 0 & -0.130 & 0.0121 \\ 0 & 0 & -81.0 & -0.130 \end{pmatrix}. \tag{20}$$

We use the usual TRANSPORT definitions; displacements are in units of cm and angles are in units of mr.

The mechanical realization of the electrostatic bend is shown in Figure 9. The electrodes are supported on Macor [11] posts between a pair of plates that define and maintain the desired geometry; the field clamps are attached to the same plates. The electrical connections are made via spring-loaded contacts. The entire assembly is fabricated with UHV- compatible materials, and is designed to be bakable to 250 C. The bend is mounted inside a vacuum can that incorporates viewscreen mechanisms and viewports to permit observation of the beam spots at the object and image points. A large port centered under the bend provides for a connection to a DI pump.

6.2 The Solenoid

The solenoids used throughout the spin manipulator are based on a design developed at SLAC for the original SLC polarized electron source [14]; it is shown in Figure 10. The agreement between POISSON [15] calculations of the axial field of the solenoid and the measured fields is quite satisfactory. In order to simplify the bakeout of the vacuum system, the solenoid was designed to be bakable to over 200 C. To accomplish this, the solenoid uses No. 14 AWG square wire [12] insulated with a double coating of polymide supplemented with 0.076 mm thick mica at the crossover points and potted using 526 Aremco-bond organic adhesive [13]. The potted coil is also wrapped using 0.5 mm thick Kapton polymide tape to provide additional insulation before it is inserted in the soft iron casing. The mechanical design of the coil and case permits the solenoid to be removed from a conflat-flanged beampipe without removing the (70 mm diameter) flanges. The solenoid coil has a total of 742 turns; when it is excited with a one ampere current it has a focal length of about 50 cm for a 100 keV electron beam.

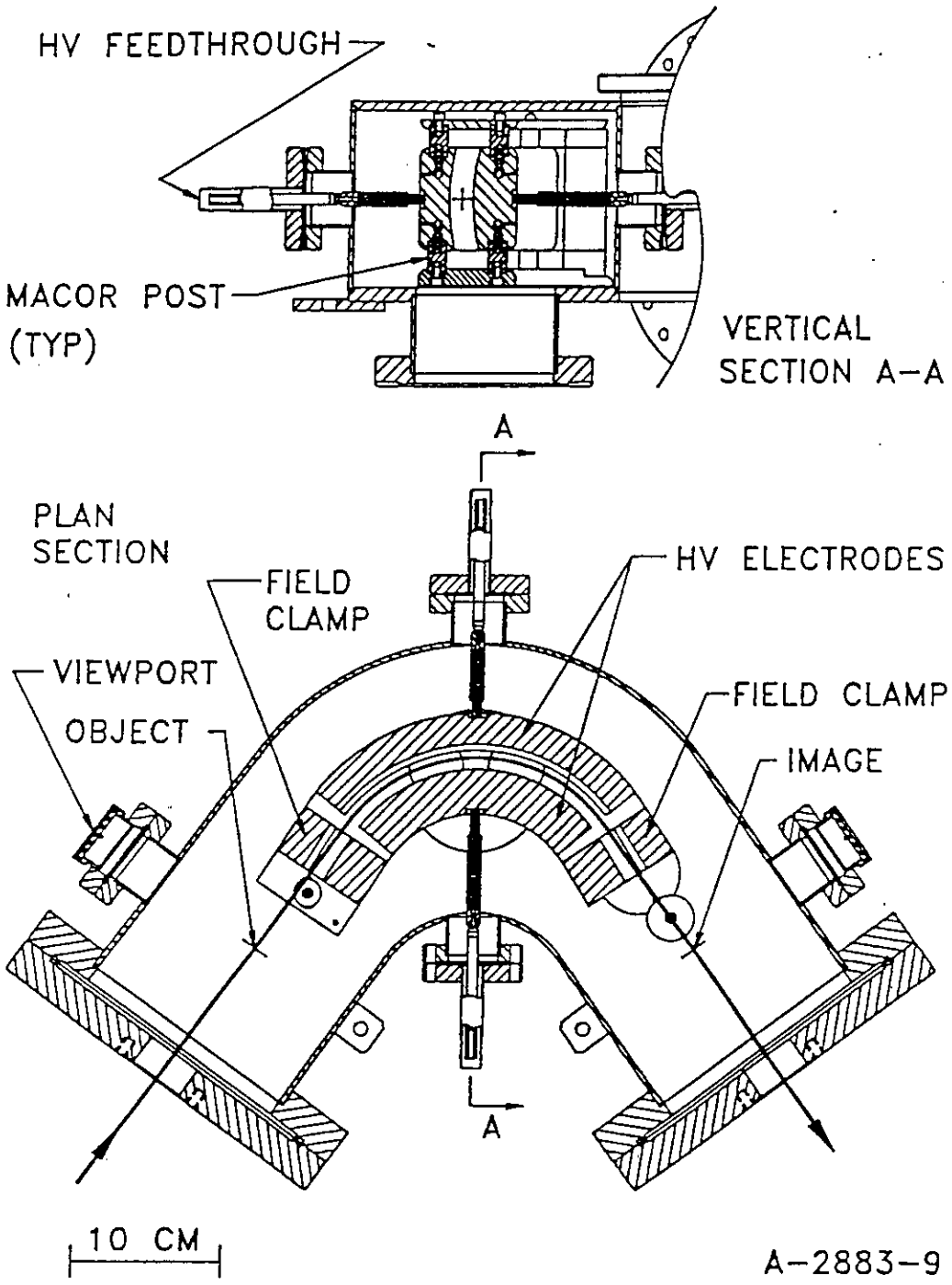

Figure 9: The mechanical construction of the electrostatic bend and its vacuum chamber.

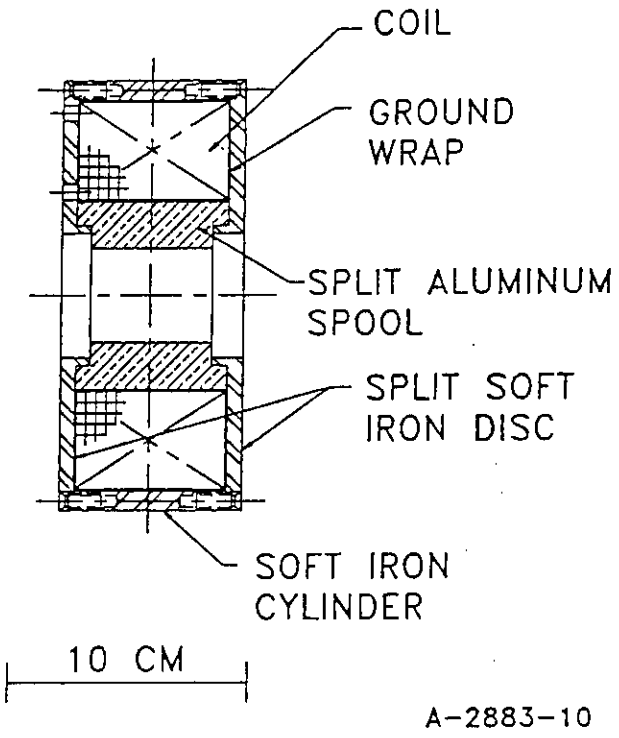

Figure 10: The construction of the bakable solenoid.

7 Operation and Performance of the "Z" Spin Manipulator

7.1 Setup of the "Z" Spin Manipulator

The setup of the "Z" spin manipulator built for the Illinois/CEBAF polarized electron source can be summarized by a pair of tuning diagrams. In Figure 11 we present the tuning diagram for the θ-rotator calculated using the TRANSPORT code. (The tuning diagram for the ϕ-rotator is quite similar.) The diagram shows the field strengths (which are proportional to the currents) required of all solenoids for any desired spin precession. Recall that each rotator has two degrees of freedom: the current of the coupled focussing solenoids; and the current of one of the precessing solenoids. The current in the other precessing solenoid is then fixed by the desired precession angle. Nevertheless, the tuning diagram shows the settings for both precessing solenoids. The sum of the two precessing solenoids, if shown, would be a straight line with a positive slope since (for identical solenoids) the precession angle is proportional to the sum of the field strengths.

Operationally, the setup is straightforward. First one sets the spin- manipulating solenoids to the values as determined from the tuning diagrams. Then one adjusts the counter-wound focusing solenoid pairs first in the θ rotator and then the ϕ rotator to

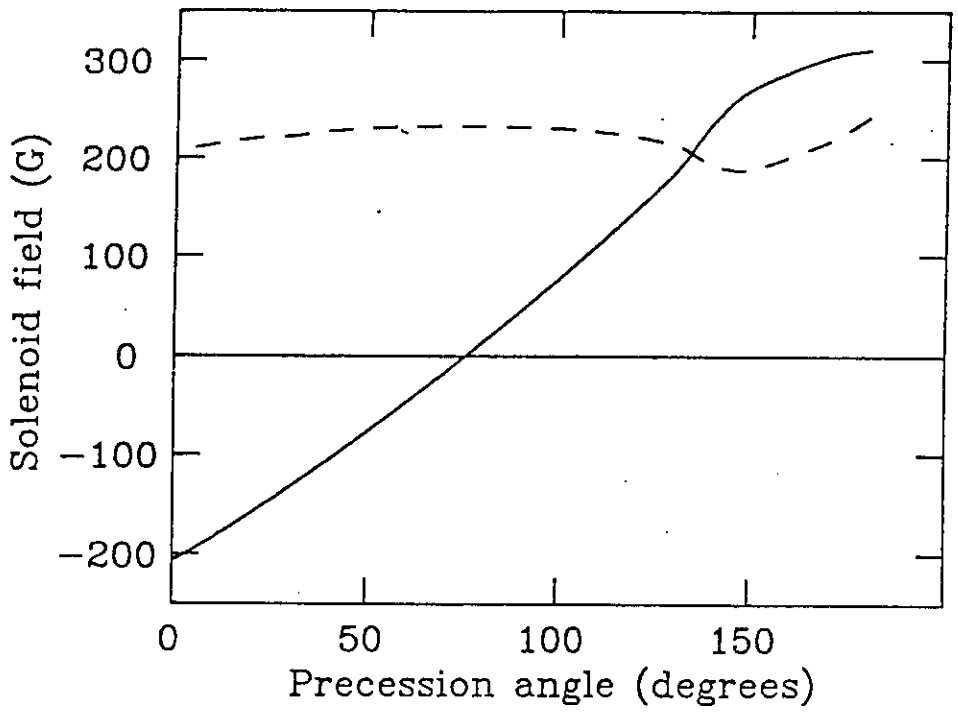

Figure 11: Tuning diagram for the solenoids controlling the θ precession. The solid curve corresponds to $S_{\theta 1a}$ settings, while the dashed curve corrsponds to $S_{\theta 1b}$ settings.

obtain waists at the entrance to the second electrostatic bend, and at the output of the system, respectively. Viewscreens are available at these locations to simplify the procedure. The values of operating currents for the solenoids obtained in this manner agree well with the values calculated using TRANSPORT.

Because the geometric alignment of all of the elements of the "Z" is not perfect, it is necessary to make small adjustments in the beam trajectory as the settings of the manipulator are changed. A number of horizontal and vertical steering coils have been added to the system to facilitate these adjustments; these coils are located at the entrance to the manipulator, and in each of the rotators both upstream and downstream of the angle-setting solenoids. A change in the setting of the θ or ϕ rotator by 90° typically results in the beam spot at the exit of the manipulator moving by a few mm; this small motion is easily corrected using the steering coils, and could probably be reduced significantly by a very careful mechanical alignment of the manipulator.

During the course of setting up the beam transport through the spin manipulator we also investigated a somewhat simpler "tune" in which the currents in the solenoid pairs that precess θ and ϕ were kept equal, rather than adjusted following the scheme summarized in the tuning diagram shown in Figure 11 and the similar diagram for the ϕ-rotator. This alternate tune proved to be quite satisfactory, and requires two fewer power supplies than the original design scheme, so it will probably be used when the manipulator is installed

at CEBAF.

7.2 Vacuum Performance

The vacuum performance of the spin manipulator has been entirely satisfactory. After an initial bakeout for about ten days at 220 C, the system pressure (as measured using the pump currents on the ion pumps beneath each electrostatic bend) was about 5×10^{-10} torr. It has remained at roughly that value or slightly better over many months of use since the bakeout. The vacuum in the polarized source after a full bakeout is $\sim 6 \times 10^{-11}$ torr when it is completely isolated by closing the main vacuum valve just below the anode. With this valve open, but the valve between the gun and the first electrostatic bend of the "Z" closed, the pressure in the source rises to $\sim 1 \times 10^{-10}$ torr. When the valve to the manipulator is opened the pressure rises further to $\sim 1.5 \times 10^{-10}$ torr. However, the "Z" provides almost complete isolation from higher pressures further downstream. In our present system the beamline is terminated in a small Faraday cup, located about 2 meters downstream of the exit to the manipulator. During recent experiments using the spin manipulator the base pressure at the source with all valves open but no beam present was 2×10^{-10} torr (we had not carried out a full bakeout). Even with a pressure of 7.5×10^{-7} torr at the Faraday cup, the pressure at the source rose only to 3.5×10^{-10} torr.

7.3 Measurements of the Performance of the "Z" Spin Manipulator

Our first use of the spin manipulator involves its use in conjunction with a Mott polarimeter to measure the polarization vs wavelength for electron beams emitted from a variety of semiconductor photocathodes. The Mott polarimeter measures polarization by taking advantage of the spin-orbit interaction in the (Mott) scattering of polarized electrons from a thin gold foil. Mott scattering measures the spin component transverse to the scattering plane. In order to insure that we measure the maximum electron polarization from the material under test, the spin manipulator must rotate the spin from its longitudinal orientation at the exit of the gun to transverse at the location of the gold scattering foil ($\theta = 90°$, $\phi = \pm 90°$). The Mott scattering chamber is located just after the spin manipulator (at the location of the waist produced by the ϕ rotator). As a check on the operation of the spin manipulator we made measurements of the transverse polarization component for two conditions: (1) set $\eta_\phi = 0°$ and vary η_θ from $-180°$ to $180°$; and (2) set η_θ at a maximum as measured in condition (1) and vary η_ϕ from $-180°$ to $180°$. For the first condition, a plot of polarization versus rotation angle should generate a sine curve, while a similar plot for the second condition should generate a cosine curve.

The results of the measurements are shown in Figure 12. The upper curve shows a plot of polarization versus η_θ for $\eta_\phi = 0°$. The rotation angle, η_θ, used for the ordinate in this plot was determined using Equation 2 and the magnetic field map data for each solenoid.

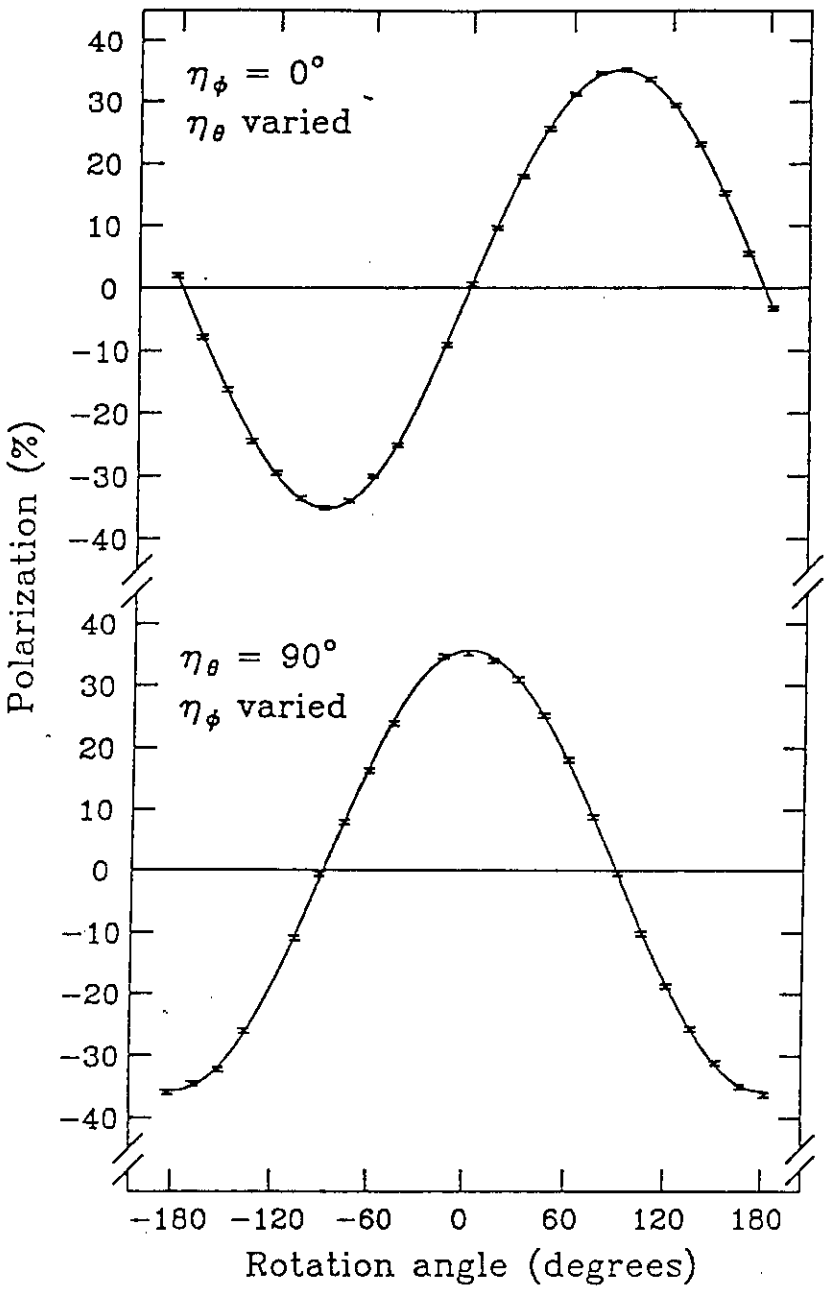

Figure 12: Tests of the operation of the "Z" spin manipulator using a Mott polarimeter.

The solid line is a fit to the observed apparent polarization (obtained in the usual way [16] from the measured scattering asymmetry in the Mott polarimeter through a measurement of the effective Sherman function) using the form $P(\theta) = P_0 \sin(k\theta + \theta_0)$. A best-fit was found with $P_0 = 35.2 \pm 0.1$, $k = 1.012 \pm 0.001$, and $\theta_0 = (0.99 \pm 0.15)°$; the overall χ^2 of the fit was 1.1 per degree of freedom. The 1.2% deviation of k from unity is well within the systematic uncertainty estimated for the field maps that were used to calculate θ; in fact, the fit to these data represents a highly precise determination of the absolute scale for the field maps. The "phase angle" $\theta_0 = 0.99°$ is consistent with the angular errors that are estimated to result from hysteresis in the fields of the solenoids and from the fact that we did not shield against the earth's magnetic field in the apparatus in order to simplify its construction and maintenance. Results for the ϕ rotation in the lower half of the figure are similarly satisfactory.

These data also provide confirmation for our estimates of the uncertainties in the spin orientation due to errors in setting the voltages and currents that control the manipulator. Typical statistical uncertainties in the measured polarizations are between 0.3% and 0.4%. The χ^2 of 1.1 per degree of freedom indicates that there are no significant additional uncertainties in the spin projection beyond those implicit in the statistical accuracy of the data. Considering the curve at the crossover points (where the projection passes through zero) we note that an error of about 0.2° in the spin direction would have caused the measured spin projection to move by a standard deviation relative to the best fit curve; no such deviations were observed.

8 Conclusions

We have shown that the optical system described in this paper, the "Z" manipulator, is capable of setting the polarization direction of a beam of polarized electrons to an arbitrary orientation relative to the beam direction. We have also demonstrated that, to a large extent, the optical behavior can be decoupled from the precession behavior. The benefit of this functional separation is a simplification of the beam line diagnostics. View screens can be placed at the positions of the waists; those positions do not shift when a different polarization direction is requested. The sensitivities of the polarization precession in the manipulator to fluctuations in the beam energy and to errors in setting the operating fields are entirely manageable, as is evidenced by the excellent quality of the Mott scattering data we have obtained using the manipulator. The transverse optical properties of the manipulator are entirely satisfactory, and it has been shown to provide excellent vacuum isolation between the polarized source and attached apparatus (well over a factor of 100). Because the spin is exactly transverse just after the first electrostatic bend, it is possible to incorporate a Mott scattering device there permanently for monitoring the operation of the source independent of the accelerator. The only obvious drawback to the "Z" design is that it is somewhat complicated to construct and it operates ideally (with complete decoupling of the θ and ϕ settings) only at a single beam energy.

Acknowledgments

This work has received support from many sources. Three of us (D.E., B.D., and L.S.C.) are supported in part by the National Science Foundation under Grant No. PHY–89-21146 and by CEBAF under Contract No. SURA-88-C8531LD. One of us (D.P.H.) is supported in part by Contract SURA-91-A9035SD with CEBAF. Finally, one of us (C.K.S.) is supported by the Department of Energy under Contract No. DE-AC05-84ER40150.

References

[1] see, eg., T. W. Donnelly and A. S. Raskin, Ann.Phys. (N.Y.) **169**, 247 (1986) and references therein.

[2] see, eg., L. S. Cardman, "Proc. the EPS Conf. on Hadronic Structure and Electroweak Interactions," Amsterdam, August 5-10, 1991 (to be published), and references therein.

[3] see, eg., M. Salomaa and H. A. Enge, Nucl. Inst. and Meth. **145**, 279 (1977).

[4] E. Reichert, as reported by C. K. Sinclair in *Proc. 8th Int. Symp. on High Energy Spin Physics*, AIP Conf. Proc. **187**, 1412, ed. K. J. Heller, (AIP, New York, 1989).

[5] E. Reichert, in *High Energy Spin Physics* **1**, 303, K.-H. Althoff and W. Meyer, eds. (Springer-Verlag, Berlin, 1991).

[6] K. L. Brown, F. Rothacker, D. C. Carey, and Ch. Iselin, SLAC 91, (1977).

[7] V. Bargman, L. Michel, and V. L. Telegdi, Physical Review Letters **2**, 435 (1959).

[8] D. Engwall, "Comparison of Wien Filter and Mainz Spin Manipulator," Univ. of Illinois Nuclear Physics Laboratory Polarized Source Technical Note # 89-5 (unpublished).

[9] H. Wollnik, T. Matsuo, and H. Matsuda, Nucl. Instr. and Meth. **102**, 13 (1972).

[10] H. Wollnik, *Optics of Charged Particles*, (Academic Press, Inc., 1987).

[11] Macor is the trademark for a machinable glass ceramic, manufactured by Corning Glass Works, Corning, NY 14830.

[12] Purchased from Magnet Wire Supply, Westlake Village, CA 91302; the double polymide coating is referred to as "HML."

[13] Available from Aremco Products, Inc., Ossining, N.Y. 10562.

[14] C. K. Sinclair and R. H. Miller, IEEE Trans. Nucl. Sci. **NS-28**, 2649 (1981).

[15] M. T. Menzel and H. K. Stokes, Los Alamos National Laboratory Report LA-UR-87-115 (unpublished).

[16] T. J. Gay and F. B. Dunning, Rev. Sci. Instr. **63**(2), 1635 (1992).